

# SED Analysis of 13 Spectroscopically Confirmed Galaxies at $z \simeq 6$ to Constrain UV-Slope, Model Dust Attenuation and Escape Fractions

JUNEHYOUNG JEON,<sup>1</sup> ROGIER A. WINDHORST,<sup>2</sup> SETH H. COHEN,<sup>2</sup> ROLF A. JANSEN,<sup>2</sup> BRENT M. SMITH,<sup>2</sup>  
TIMOTHY CARLETON,<sup>2</sup> EIICHI EGAMI,<sup>3</sup> KRISTIAN FINLATOR,<sup>4</sup> LINHUA JIANG,<sup>5</sup> KARTHEIK G. IYER,<sup>6</sup> AND VIHANG MEHTA<sup>7</sup>

<sup>1</sup>*Department of Astronomy, University of Texas, Austin, TX 78712, USA*

<sup>2</sup>*School of Earth & Space Exploration, Arizona State University, Tempe, AZ 85287-1404, USA*

<sup>3</sup>*Steward Observatory, University of Arizona, 933 North Cherry Avenue, Tucson, AZ 85721, USA*

<sup>4</sup>*New Mexico State University, Las Cruces, NM 88003, USA*

<sup>5</sup>*Kavli Institute for Astronomy and Astrophysics, Peking University, Beijing 100871, China*

<sup>6</sup>*Dunlap Institute, University of Toronto, Toronto, ON, Canada*

<sup>7</sup>*Minnesota Institute for Astrophysics, University of Minnesota, 116 Church Street SE, Minneapolis, MN 55455, USA*

## ABSTRACT

The reionization of the hydrogen in the Universe is thought to have completed by redshift  $z \simeq 5.5-6$ . To probe this era, galaxy observations in the Subaru Deep Field (SDF) have identified more than 100 galaxies at  $z \simeq 6$ , many spectroscopically confirmed through follow-up observations. We model the spectral energy distributions (SEDs) of 13 SDF galaxies with the CIGALE and Dense Basis codes using available optical/IR data. Modeling deep IR photometry has the potential to constrain the galaxy's Lyman continuum (LyC) escape fraction ( $f_{\text{esc}}$ ). We use the modeled nebular emission lines and find that the implied escape fractions ranges from **0 to 0.8 with a median of  $\sim 0.35$  for Dense Basis and  $\sim 0.55$  for CIGALE**. Significant uncertainties in the data exist, so that fitting results in a large range of  $f_{\text{esc}}$  for individual objects. The implied median  $f_{\text{esc}}$ -values may be high enough for galaxies to finish reionization by  $z \sim 6$ . Furthermore, we find no strong trends between the UV-slope  $\beta$  or  $E_{\text{B}-\text{V}}$  with model  $f_{\text{esc}}$ . If true, the lack of trends suggest that other factors besides nebular emission or dust extinction could have led to LyC escaping, such as the presence of holes in the ISM with sufficiently wide opening angles from outflows of supernovae and/or weak AGN, resulting in a range of implied  $f_{\text{esc}}$ -values depending on the viewing angle of each galaxy. The current *HST*, *Spitzer* and ground-based photometric and model errors for the galaxies remain large, so IR spectroscopic observations with the *James Webb Space Telescope* are needed to constrain this possibility.

**Keywords:** High-Redshift Galaxies — Spectral Energy Distributions — Interstellar Dust Extinction — Reionization

## 1. INTRODUCTION

Detailed studies of high redshift galaxies observed in the first billion years have provided a wealth of information about early galaxy formation and evolution. Developments in ground- and space-based telescopes, such as the availability of very wide-field cameras on 8 to 10m class telescopes and medium- or narrow-band filters that fall between the worst sky lines, enabled the identification of numerous high redshift galaxies (*e.g.*, Ellis et al. 2013; Jiang et al. 2013; Bouwens et al. 2015; Ota et al.

2017; Finkelstein et al. 2019; Hu et al. 2019). In particular, observations with the Subaru telescope, *HST*, and the *Spitzer Space Telescope* have discovered numerous high redshift galaxies in optical, near-IR, and mid-IR, respectively (*e.g.*, Yan et al. 2010; Lorenzoni et al. 2011; McLure et al. 2011; Kashikawa et al. 2011; Trenti et al. 2011). Large areas of sky have been imaged from the ground with these narrow-band filters, and the detected narrow-band emission of some of the brighter galaxies have been spectroscopically confirmed to be Lyman  $\alpha$  ( $\text{Ly}\alpha$ ) emission (*e.g.*, Finkelstein et al. 2013; Jiang et al. 2013; Konno et al. 2014; Jiang et al. 2016; Laporte et al. 2017; Stark et al. 2017; Ouchi et al. 2018). The *James Webb Space Telescope* (*JWST*), which can access wave-

lengths presently inaccessible with *Hubble Space Telescope* (*HST*) and that are difficult to access from the ground due to Earth’s atmosphere, will be able to observe these objects at higher resolution to identify AGN, star-formation regions, and outflows (*e.g.*, Gardner et al. 2006; Maseda et al. 2019; Windhorst et al. 2018). As reionization of the intergalactic hydrogen in the Universe is thought to have been completed by  $z \simeq 5.5 - 6$  (*e.g.*, Keating et al. 2020), such high redshift galaxies can help us study this interesting period.

Some parameters of these high redshift galaxies useful for studying the epoch of reionization include the UV-continuum slope ( $\beta$ ), which can help constrain the characteristics of their young stellar populations (such as age Conroy 2013; Jiang et al. 2020), their Lyman Continuum (LyC) escape fraction ( $f_{\text{esc}}$ ) which provides a measure of how much energy was available for reionization (*e.g.*, Miralda-Escudé et al. 2000; Loeb & Barkana 2001; Barrow et al. 2020), and the  $E_{\text{B-V}}$  reddening values (*e.g.*, Calzetti et al. 2000; Meurer et al. 1999), which are a measure of their internal attenuation by dust.  $E_{\text{B-V}}$  or  $\beta$  may be correlated with  $f_{\text{esc}}$ , given that  $\beta$  is related to the amount of ionizing emission originating from the galaxy, and  $E_{\text{B-V}}$  is related to the amount of dust and gas preventing that emission from escaping the galaxy (*e.g.*, Ono et al. 2010; Hayes et al. 2011).

Previous studies have suggested that a minimum escape fraction of  $\sim 20\%$  is needed to finish the reionization of the hydrogen in the Universe at  $z \simeq 6$ , assuming UV-bright sources ( $M_{\text{AB}} \lesssim -21$  mag) dominate reionization (*e.g.*, Finkelstein et al. 2012; Robertson et al. 2015; Naidu et al. 2020). However, it is unclear what  $f_{\text{esc}}$ -values are typical for  $z \simeq 6$  galaxies. For galaxies at  $z < 4$ , escape fraction may be directly measured through rest-frame UV imaging and/or spectroscopy. For galaxies at high redshift like those in our sample, such direct methods do not work, since a larger portion of LyC photons are absorbed by the higher HI fraction in the IGM at  $z > 4$ , and any constraints must rely on the more limited IR data that are available for our galaxies (Bian & Fan 2020).

Hence, we turned to an alternative method of SED fitting to infer the escape fraction of our high redshift galaxies. Previous studies have noted that modeling nebular emission is crucial in producing accurate SED models, particularly at high  $z$  (*e.g.*, Schaerer & de Barros 2009; Jiang et al. 2016). This is related to  $f_{\text{esc}}$ , since significant nebular emission is indicative of ionizing photons exciting the gas to produce rest-frame UV and optical emission lines instead of escaping the galaxy, implying lower  $f_{\text{esc}}$ -values. Thus, SED modeling can be used to *indirectly* constrain the fraction of ionizing pho-

tons that is not absorbed and reprocessed as emission lines, but instead escapes from galaxies.

Moreover, several authors found unusually blue  $\beta$  values as steep as  $\beta \simeq -2 \sim -3$  for faint galaxies at  $z \geq 6$  using photometric methods (*e.g.*, Bouwens et al. 2014; Labbé et al. 2010; Jiang et al. 2020). To see how such surprisingly blue slope parameters might occur, SED modeling — which previously has been used to characterize galaxy populations at low (Papovich et al. 2001; Shapley et al. 2001, 2005) and moderate redshifts (Ono et al. 2010) — can be used to interpret the UV-slope  $\beta$ .

To perform this modeling on a large number of galaxies in the Subaru Deep Field (SDF), 67 candidate galaxies at  $z \simeq 6$  were identified in Jiang et al. (2013)<sup>1</sup> to be the most luminous galaxies in Ly $\alpha$  emission and/or in UV-continuum in this redshift range around  $z \simeq 6$ . Of these galaxies, 7 were chosen to have particularly blue  $\beta$  and were imaged by *HST* Wide Field Camera 3 (WFC3) in the F105W, F110W, F125W, and F160W filters, and their rest-frame UV SEDs were modeled with the CIGALE program (Boquien et al. 2019), as described in detail in Jiang et al. (2020, hereafter J20).

In this paper, we study the SEDs of **13 galaxies with available near-IR data, including 1 galaxy from J20**, and compare these samples. Our goal for this comparison is to determine if, and to what extent, galaxy parameters are correlated with LyC escape fraction, and how galaxy properties are related to the slope of the UV continuum. We use the CIGALE code for our SED models, which was also used by J20 for their sample of galaxies. In addition, we performed SED fitting using the Dense Basis code (Iyer & Gawiser 2017) to ensure that our results were not sensitive to the particular SED-fitting code applied. For all 13 SDF galaxies, we not only fit the stellar age, but also explore the values of the LyC escape fraction ( $f_{\text{esc}}$ ) and dust extinction ( $E_{\text{B-V}}$ ) allowed for each galaxy to determine their best SED fit. This paper thus presents the SED models of the **13**  $z \simeq 6$  galaxies in the SDF that have near-IR data to possibly constrain their escape fraction. We further discuss the range of SED parameter values permitted by the CIGALE and Dense Basis models.

The paper is organized as follows. In section 2, we describe all available data for these  $z \simeq 6$  galaxies, as well as archival UKIRT/WFCAM K-band data. In section 3, we describe how the SED modeling of the galaxies was

<sup>1</sup> Five of the spectroscopically confirmed galaxies are not in the SDF, but rather the UKIDSS Ultra-Deep Survey (UDS), with WFC3-IR coverage from the Cosmic Assembly Near-infrared Deep Extragalactic Legacy Survey (CANDELS; Grogin et al. 2011; Koekemoer et al. 2011)

performed, and describe the results. In section 4, we discuss constraints to the implied  $f_{\text{esc}}$ ,  $\beta$ , and  $E_{\text{B-V}}$  values for the sample of 13 SDF galaxies at  $z \simeq 6$  and investigate possible trends. We then summarize our results in section 5. All AB magnitudes from J20 were converted to mJy to facilitate direct modeling with the CIGALE and Dense Basis programs (Oke & Gunn 1983). They are presented as  $\mu\text{Jy}$  in this paper.

## 2. OVERVIEW OF EXTANT GALAXY DATA USED

Table 1 lists IDs, coordinates, redshifts, and measured fluxes of the 13 galaxies in our sample as given in Jiang et al. (2013, 2016) and J20. **We also include the UV-slope measurements for the the galaxy from J20, ID43.** *HST*/WFC3 images in the F105W, F110W, F125W, and/or F160W filters are available in various combinations for all 13 galaxies, and our sample also has *Spitzer*/IRAC imaging available in the SDF, or from the larger area covered by the Subaru XMM-Newton Deep Survey (Furusawa et al. 2008) from Jiang et al. (2013, 2016). Sub-pixel dithering was performed to improve the Point Spread Function (PSF) sampling (Jiang et al. 2013). For the optical *HST* images, photometry was performed using SExtractor (Bertin & Arnouts 1996) adopting a  $2''$  diameter circular aperture and subtracting the local background. We applied an aperture correction based on bright point sources within the same image to account for any light losses outside each object aperture. Rather than homogenizing PSFs to a given value, PSF matching was done by multiplying the weight maps by the inverse square of the PSF Full Width at Half Maximum (FWHM). For the infrared images, we used SExtractor with a Kron factor of 1.8 to determine the total magnitudes, and the same aperture corrections were applied.

**For the IRAC 3.6 and 4.5  $\mu\text{m}$  data, Jiang et al. (2016) deblended sources first by modeling the brightest neighbors of the source with iGALFIT (Ryan 2011), convolving with the PSF image, and then subtracting the neighbors from the image.** Photometry was then done on a  $1''.8$  radius aperture with an aperture correction of 0.4 mag (Jiang et al. 2016).

Since CIGALE provides SED models into the observed infrared regime, we searched the *Herschel* archive for images of the galaxies to possibly constrain their dust content. In the region of the SDF containing our 13 galaxies, extant *Herschel* far-IR observations are too shallow for robust detections of any of our sample galaxies. Hence, we have no far-IR data to place further constraints on thermal dust emission in our CIGALE modeling.

To obtain the K-band data for the galaxies of J20, we searched the WFCAM Science Archive<sup>2</sup>. After identifying the exposures containing each of the galaxies, we used the DS9 program (Joye & Mandel 2003) to analyze the K-band image files from LAS or UDS. We selected a circular region around the location of each galaxy and a circular region of background sky devoid of object signal, their sizes based on the resolution of each image, to estimate the source and background flux measurements on the Vega magnitude system, given the zero-point of Hodgkin et al. (2009). Using the region analysis function of the DS9 program, the sum of the pixel values in the regions were used to measure the flux, and the standard deviation of the background pixel values was used to estimate the uncertainties of the flux values. For the K-band, we used the conversion from Vega to AB magnitudes from Hewett et al. (2006). We converted the apparent AB-magnitude values to  $\mu\text{Jy}$  units (Oke & Gunn 1983).

Deep observations as part of the UKIRT WFCAM Large Area Survey (LAS) or the Ultra Deep Survey (UDS) presented in Lawrence et al. (2007) observed the SDF galaxies of J20 in the K-band, and provided 2.2  $\mu\text{m}$  flux measurement or upper limits. In those cases, the galaxies have 5–6 independent flux measurements to constrain the range of implied physical parameters allowed by the CIGALE models. **Out of the 67 SDF galaxies including the 7 analyzed by J20,** 14 galaxies did not have any reliable flux measurements. An additional 6 galaxies only had one reliable flux measurement, so they were also omitted. We also omitted 4 galaxies that had neither K-band nor IRAC measurements — *i.e.*, no measurements beyond 2  $\mu\text{m}$  — which did not allow meaningful modeling of their escape fractions. In the end, the K-band data was not used for these galaxies, since it did not improve the modeling of the 7 galaxies significantly. **Finally, we rejected 2 galaxies with signal to noise greater than 3 in the IRAC1 data, 15 galaxies with only an lower limit on the *Spitzer* data, 9 galaxies with nearby neighbors within 1.7–2.0'' IRAC beam in the HST images, and 4 galaxies that did not readily have images that we could check for neighbors.** Thus, 13 galaxies could be modeled by CIGALE out of the full sample of 67 SDF galaxies. The visual cutouts of the galaxies can be found in Jiang et al. (2013).

<sup>2</sup> <http://wsa.roe.ac.uk/>

**ID43** was observed in the UKIRT WFCAM LAS with shallow observations. A  $2\sigma$  upper limit to the K-band fluxes is therefore listed for ID43 in Table 1.

Table 1. High redshift galaxy flux data at various *HST* and *Spitzer* filters with measured UV-slope from J20

ID	R.A.	Decl.	z	Slope	$z'$	$y'$	F105W	F110W	F125W	F160W	IRAC 1	IRAC 2	K
(1)	(2)	(3)	(4)	(5)	(6)	(7)	(8)	(9)	(10)	(11)	(12)	(13)	(14)
	J2000.0	J2000.0		$\beta$	$\mu\text{Jy}$	$\mu\text{Jy}$	$\mu\text{Jy}$	$\mu\text{Jy}$	$\mu\text{Jy}$	$\mu\text{Jy}$	$\mu\text{Jy}$	$\mu\text{Jy}$	$\mu\text{Jy}$
ID03	13:24:16.468	+27:19:07.65	5.665	...	$0.331 \pm 0.012$	$0.353 \pm 0.026$	...	$0.291 \pm 0.011$	...	$0.286 \pm 0.018$	$0.334 \pm 0.065$	$0.254 \pm 0.077$	...
ID15	13:24:23.705	+27:33:24.82	5.710	...	$0.492 \pm 0.014$	$0.461 \pm 0.025$	...	$0.501 \pm 0.014$	...	$0.409 \pm 0.023$	$0.879 \pm 0.057$	$0.698 \pm 0.071$	...
ID20	13:24:40.527	+27:13:57.91	5.734	...	$0.119 \pm 0.012$	$0.113 \pm 0.028$	...	...	$0.139 \pm 0.012$	$0.138 \pm 0.014$	$0.302 \pm 0.083$	...	...
ID23	13:24:18.450	+27:16:32.56	5.922	...	$0.244 \pm 0.011$	$0.198 \pm 0.025$	...	...	$0.213 \pm 0.010$	$0.201 \pm 0.013$	$0.328 \pm 0.048$	...	...
ID24	13:25:19.463	+27:18:28.51	6.002	...	$0.244 \pm 0.011$	$0.198 \pm 0.025$	...	$0.213 \pm 0.010$	...	$0.201 \pm 0.013$	$0.328 \pm 0.048$	...	...
ID25	13:24:26.559	+27:15:59.72	6.032	...	$0.291 \pm 0.013$	$0.281 \pm 0.026$	...	$0.164 \pm 0.018$	...	$0.209 \pm 0.021$	$0.692 \pm 0.045$	$0.592 \pm 0.071$	...
ID27	13:24:10.766	+27:19:03.95	6.040	...	$0.086 \pm 0.012$	...	...	...	$0.098 \pm 0.010$	$0.069 \pm 0.012$	$0.191 \pm 0.053$	...	...
ID31	13:23:45.632	+27:17:00.53	6.112	...	$0.334 \pm 0.012$	...	...	$0.116 \pm 0.015$	...	$0.100 \pm 0.017$	$0.344 \pm 0.063$	...	...
ID34	13:23:45.757	+27:32:51.30	6.315	...	$0.219 \pm 0.012$	$0.350 \pm 0.026$	...	...	$0.398 \pm 0.015$	$0.398 \pm 0.015$	$1.076 \pm 0.089$	...	...
ID35	13:24:40.643	+27:36:06.94	6.332	...	$0.219 \pm 0.012$	...	...	...	$0.240 \pm 0.013$	$0.225 \pm 0.015$	$1.854 \pm 0.09$	$1.159 \pm 0.117$	...
ID43	13:23:53.054	+27:16:30.75	6.542	$-3.39 \pm 0.41$	$0.102 \pm 0.012$	$0.139 \pm 0.027$	$0.152 \pm 0.018$	...	$0.111 \pm 0.007$	$0.087 \pm 0.009$	$0.275 \pm 0.061$	...	$<0.263$
ID54	13:24:08.313	+27:15:43.49	6.556	...	$0.163 \pm 0.012$	$0.219 \pm 0.026$	...	...	$0.150 \pm 0.019$	$0.171 \pm 0.024$	$0.319 \pm 0.073$	$0.299 \pm 0.010$	...
ID62	13:23:59.766	+27:24:55.75	6.964	...	$0.058 \pm 0.016$	$0.394 \pm 0.033$	...	$0.229 \pm 0.008$	$0.247 \pm 0.011$	$0.242 \pm 0.011$	$0.421 \pm 0.062$	$0.310 \pm 0.060$	...

NOTE—The ID numbers are from Table 1 in Jiang et al. (2013). The  $z'$ - and  $y'$ -band fluxes are from Jiang et al. (2013), and the remainder from Jiang et al. (2016, 2020). The  $\beta$  value is also from J20. Some galaxies do not have measurements in some of the filters, so those columns are left empty.



(predominantly OIII and H $\alpha$ ), and that those are at IRAC wavelengths at these redshifts

### 3. SED MODELING

The Lyman-continuum escape fraction may be constrained by the implied presence of emission lines in the SED of galaxies. A stellar population produces a certain number of ionizing photons based on its age and stellar mass. If none of those photons escape ( $f_{\text{esc}}=0$ ), then the energy will be reprocessed in the ISM, producing strong emission lines. If the escape fraction is high ( $f_{\text{esc}} \gtrsim 0.3$ ), there will be no associated emission lines (e.g., [Smith et al. 2018, 2020](#); [Steidel et al. 2018](#)). CIGALE uses the modeled stellar age and stellar mass to determine the expected emission line strength, which may be many Angstroms in equivalent width for these very young stellar populations, and predicts the associated emission line strengths for a given  $f_{\text{esc}}$ -value. If the near-IR photometry at the emission line wavelengths is brighter than the CIGALE models predict, then the presence of stronger emission line is implied, suggesting lower  $f_{\text{esc}}$ -values, and vice-versa. Ultimately, because of uncertainties in the measured stellar population parameters, near-IR photometry, **which are at OIII and H $\alpha$  lines for redshifts of our galaxies**, is only weakly dependent on  $f_{\text{esc}}$ , resulting in larger errors in the implied  $f_{\text{esc}}$ -values. Deep multi-band photometry including the *Spitzer* IRAC 3.6–4.5  $\mu\text{m}$  images may thus place some meaningful constraints on the allowed  $f_{\text{esc}}$ -values for these 13 galaxies, enabling us to explore the average  $f_{\text{esc}}$ -value range for galaxies at this redshift, and search for any trends that may exist between  $f_{\text{esc}}$  and other galaxy properties.

Therefore, we used the CIGALE to perform SED modeling for all our SDF galaxies. We also used the broad-band fluxes from [Jiang et al. \(2016, 2020\)](#) for CIGALE fitting, as described in § 2. **CIGALE models fit the Ly $\alpha$  line with a fixed escape fraction directly related to the restframe nebular lines. Despite the uncertainties in Ly $\alpha$  emission modeling, one goal of this paper is to constrain escaping Ly $\alpha$  emission in high redshift galaxies. Therefore, we include the  $z'$  photometry which contains important information regarding the strength of escaping Ly $\alpha$  emission relative to other emission lines and keep the Ly $\alpha$  line in our modeling, but increase the uncertainties of WFCAM Z and Y bands by 20 and 10%, respectively, according to the contribution of Ly $\alpha$  to these bands as listed in [J20](#). Our results and conclusions so will be under the assumption that Ly $\alpha$  has been accounted for.**

Following [J20](#), we sampled the model ages between 10 to 900 or 800 Myr using a fixed log scale with increments of 15, 25, 50, 100, and 200 for redshifts  $z > 6.0875$  and  $z < 6.0875$ , respectively, so as to not exceed the age of the Universe at each redshift. We sampled the escape fraction from 0 to 1 in steps of 0.1. The metallicity values sampled were 0.0001, 0.0004, 0.004, 0.008, 0.02, and 0.05. The  $E_{B-V}$  values we sampled were between 0 and 0.7 mag using a [Calzetti et al. \(2000\)](#) extinction curve. AGN models were not tested since no significant change was observed in the models by allowing the presence of a weak AGN in [J20](#). **Lastly, the most relevant part of the modeling is the nebular emission, which is parametrized by escape fraction and ionization parameter. We varied the ionization parameter between -1.0 and -4.0 in steps of 1 in our modeling.**

For all of our SEDs, we assumed a [Calzetti et al. \(2000\)](#) extinction law. A discussion of the possible evolution in metallicity and dust extinction is given by e.g., [Kim et al. \(2017\)](#). [Smith et al. \(2020\)](#) and [Oesch et al. \(2013\)](#), suggesting that SMC extinction curves may provide a better fit to the SED of star-forming galaxies at  $z \simeq 2.3 - 3.5$ . However, we found no significant change in the best-fit SED models when using the SMC extinction curve for our SDF sample at  $z \simeq 6$ . Fig. 1 presents the SED models of all 13 galaxies by CIGALE.

Dense Basis modeling also used [Calzetti et al. \(2000\)](#) extinction law, and model parameters such as SFR or  $f_{\text{esc}}$  were fit to match the observations instead of testing various values and determining the goodness of fit. Most galaxy models showed ages greater than 100 Myr and small values of the extinction, which is consistent with the results of [Jiang et al. \(2016\)](#), where the SED models were done with GALEV ([Kotulla et al. 2009](#)).

Rather than reporting the best-fit values from this analysis (which do not capture the uncertainties associated with this model fitting well) we report Bayesian average values and uncertainties associated with each parameter, as described in [Noll et al. \(e.g., 2009\)](#). CIGALE computes such uncertainties by taking the average value and standard deviation of the fit to be the average and standard deviation of all models, weighted by the p-value associated with the model's  $\chi^2$  value. These values give a much more comprehensive picture of the fit than only the best-fit values as it accounts for the variation in each model rather than considering only one.

One potential concern related to our SED modeling is whether objects with observations in only one IRAC band would still allow for meaningful measurements of  $f_{\text{esc}}$  with our method. To test this, we investigated the

**Table 2.** Best-fit parameters and  $\chi^2$  values of the 11 galaxies using both IRAC bands

ID	Reduced $\chi^2$	Slope	Metallicity	Age	Escape fraction	$E_{B-V}$
		$\beta$	Z	Myr		mag
(1)	(2)	(3)	(4)	(5)	(6)	(7)
ID03	0.29	$-2.41 \pm 0.15$	$0.007 \pm 0.012$	$210 \pm 180$	$0.56 \pm 0.30$	$0.1 \pm 0.1$
ID15	0.17	$-2.25 \pm 0.14$	$0.007 \pm 0.009$	$455 \pm 228$	$0.47 \pm 0.32$	$0.0 \pm 0.10$
ID25	3.26	$-2.09 \pm 0.14$	$0.005 \pm 0.005$	$667 \pm 167$	$0.14 \pm 0.20$	$0.1 \pm 0.1$
ID35	4.80	$-1.21 \pm 0.15$	$0.007 \pm 0.008$	$567 \pm 177$	$0.40 \pm 0.32$	$0.6 \pm 0.1$
ID54	0.48	$-2.07 \pm 0.22$	$0.012 \pm 0.016$	$398 \pm 245$	$0.49 \pm 0.31$	$0.0 \pm 0.1$
ID62	1.11	$-2.26 \pm 0.17$	$0.013 \pm 0.016$	$345 \pm 183$	$0.52 \pm 0.31$	$0.0 \pm 0.1$

NOTE—The model parameters along with their Bayesian error ranges of the 6 galaxies with both IRAC bands included in the fitting.

**Table 3.** Best-fit parameters and  $\chi^2$  values of the 11 galaxies with both IRAC bands modeled without IRAC2 at  $4.5\mu\text{m}$ 

ID	Reduced $\chi^2$	Slope	Metallicity	Age	Escape fraction	$E_{B-V}$
		$\beta$	Z	Myr		mag
(1)	(2)	(3)	(4)	(5)	(6)	(7)
ID03	0.20	$-2.35 \pm 0.16$	$0.007 \pm 0.012$	$261 \pm 211$	$0.50 \pm 0.31$	$0.1 \pm 0.1$
ID15	0.10	$-2.16 \pm 0.16$	$0.006 \pm 0.009$	$490 \pm 225$	$0.46 \pm 0.32$	$0.0 \pm 0.1$
ID25	3.91	$-2.12 \pm 0.18$	$0.006 \pm 0.005$	$656 \pm 173$	$0.14 \pm 0.19$	$0.1 \pm 0.1$
ID35	2.43	$-1.08 \pm 0.08$	$0.006 \pm 0.005$	$705 \pm 134$	$0.36 \pm 0.30$	$0.7 \pm 0.03$
ID54	0.60	$-2.08 \pm 0.28$	$0.012 \pm 0.016$	$365 \pm 244$	$0.49 \pm 0.32$	$0.0 \pm 0.2$
ID62	4.98	$-2.22 \pm 0.19$	$0.012 \pm 0.016$	$353 \pm 185$	$0.52 \pm 0.31$	$0.0 \pm 0.1$

NOTE—The model parameters along with their Bayesian error ranges of the same 6 galaxies as in Table 2, but modeled without using the IRAC  $4.5\mu\text{m}$  band.

**6 objects from our sample of 13 galaxies with observations in both IRAC bands.** For these objects, we modeled the SEDs both including and excluding the  $4.5\mu\text{m}$  band photometry. The results of this are shown in Tables 2 and 3, as well as Fig. 2. Because of the large uncertainties in the  $4.5\mu\text{m}$  band photometry, excluding the IRAC2 band photometry — when available — in the modeling did in general not significantly affect the inferred model parameters. More than half the galaxies overlapped in their implied values for each parameter using the two sets of models. Thus, we kept the objects without  $4.5\mu\text{m}$  observations in our final sample as long as the remainder data was of sufficient quality.

To further test whether CIGALE could constrain nebular emission without the IRAC2 band filters, we created simulated models with CIGALE with a known escape fraction between 0 and 1 for the available filters. The produced flux values were then rescaled to match our galaxy data, and 100 random variations for each

input escape fraction were produced within the uncertainty of our photometric uncertainties. The variations were then refit with CIGALE using all bands except the IRAC2 and K-band filters. The comparison between the original input escape fraction and refitted output escape fraction are presented in Fig. 3, along with a linear regression fit between the input and output  $f_{\text{esc}}$ -values. It can be seen that, while CIGALE does not exactly follow the input and output escape fractions, excluding the IRAC2 or the K band does not change the output  $f_{\text{esc}}$  compared to when all bands are included. The same procedure was repeated in Fig. 3b for Dense Basis. Both panels show similar but not identical relationships between the input and output  $f_{\text{esc}}$ -values with somewhat non-unity slopes. We use the plotted linear regression fits to map the most likely output  $f_{\text{esc}}$ -values onto the input  $f_{\text{esc}}$ -values for both CIGALE and Dense Basis, thus correcting the output from both modeling methods for this bias. Thus, the emission and  $f_{\text{esc}}$  may be con-

**Table 3.** 13 SDF galaxy data

ID	Reduced $\chi^2$	Slope	Metallicity	Age	Escape fraction	$E_{B-V}$
		$\beta$	Z	Myr		mag
(1)	(2)	(3)	(4)	(5)	(6)	(7)
ID03	0.29	$-2.41 \pm 0.15$	$0.007 \pm 0.012$	$210 \pm 180$	$0.56 \pm 0.30$	$0.1 \pm 0.10$
ID15	0.17	$-2.25 \pm 0.14$	$0.007 \pm 0.009$	$455 \pm 228$	$0.47 \pm 0.32$	$0.0 \pm 0.10$
ID20	0.04	$-1.80 \pm 0.26$	$0.013 \pm 0.017$	$345 \pm 239$	$0.49 \pm 0.32$	$0.4 \pm 0.2$
ID23	0.02	$-2.26 \pm 0.15$	$0.011 \pm 0.014$	$414 \pm 236$	$0.41 \pm 0.30$	$0.0 \pm 0.1$
ID24	0.03	$-2.31 \pm 0.13$	$0.010 \pm 0.014$	$435 \pm 235$	$0.31 \pm 0.26$	$0.0 \pm 0.1$
ID25	3.26	$-2.09 \pm 0.14$	$0.005 \pm 0.005$	$667 \pm 167$	$0.14 \pm 0.20$	$0.1 \pm 0.1$
ID27	0.48	$-2.20 \pm 0.24$	$0.007 \pm 0.012$	$404 \pm 246$	$0.45 \pm 0.31$	$0.1 \pm 0.1$
ID31	5.72	$-2.59 \pm 0.11$	$0.000 \pm 0.001$	$381 \pm 285$	$0.03 \pm 0.06$	$0.0 \pm 0.01$
ID34	0.04	$-1.64 \pm 0.20$	$0.008 \pm 0.011$	$413 \pm 235$	$0.47 \pm 0.32$	$0.4 \pm 0.1$
ID35	4.80	$-1.21 \pm 0.15$	$0.007 \pm 0.008$	$567 \pm 177$	$0.40 \pm 0.32$	$0.6 \pm 0.1$
ID43	1.02	$-2.28 \pm 0.24$	$0.005 \pm 0.007$	$443 \pm 246$	$0.39 \pm 0.31$	$0.0 \pm 0.1$
ID54	0.48	$-2.07 \pm 0.22$	$0.012 \pm 0.016$	$398 \pm 245$	$0.49 \pm 0.31$	$0.0 \pm 0.1$
ID62	1.11	$-2.26 \pm 0.17$	$0.013 \pm 0.016$	$345 \pm 183$	$0.52 \pm 0.31$	$0.0 \pm 0.1$

NOTE—The best-fit parameters and Bayesian values with errors for implied  $f_{\text{esc}}$  and UV-slope  $\beta$  for the 13 galaxies.



strained by CIGALE or Dense Basis without IRAC2 or K-band data, which is the case for a part of our sample.

Fig. 4 and 5 present the model parameters corrected for above bias. The two figures also include plots where the Dense Basis code (Iyer & Gawiser 2017) was used instead of CIGALE to determine their escape fractions to better check for SED fitting bias in CIGALE. The  $f_{\text{esc}}$  values are corrected for the model bias using the linear regression found in Fig. 3. Table 3 show the results from a Bayesian treatment of the model parameters of Fig. 1 and list uncertainties that are needed for the subsequent analysis.

Fig. 4 shows the distributions of the implied UV-slope  $\beta$ , escape fraction  $f_{\text{esc}}$ , and extinction values  $E_{B-V}$ . The  $f_{\text{esc}}$  and  $\beta$  values are from the Bayesian values, while  $E_{B-V}$  values are the best-fit  $\chi^2$  minimized values. This is because CIGALE uses the  $z = 0$  slope of the  $E_{B-V}$  vs.  $\beta$  relation from the Calzetti et al. (2000) and Meurer et al. (1999) relations (with an intercept to be determined as a free parameter from the SED fitting) to estimate  $E_{B-V}$  for a given  $\beta$ -value, and so deriving both  $E_{B-V}$  and  $\beta$  Bayesian values fully independently is not possible with this method. The CIGALE models do imply that the intercept at  $z = 6$  of the Calzetti/Meurer  $E_{B-V}$  vs.  $\beta$  relation at  $z = 0$  needs to be  $\sim 0.4$  bluer in  $\beta$  than at  $z=0$  (while adopting the same slope), which is visible in Fig. 5a.

The cumulative Gaussian probability distributions are shown for bluer galaxies ( $\beta < -2.35$ ) and redder galaxies ( $\beta \geq -2.35$ ) in the left and right panels of Fig. 4, respectively. Dense Basis suggest a total range of possible  $f_{\text{esc}}$ -values between 0–0.8. Including the  $f_{\text{esc}}=0$  values at the bottom axes of Fig. 5b, c, d, and e, the median escape fraction of CIGALE is about  $f_{\text{esc}} \sim 0.55$ , while median escape fraction of Dense Basis is about  $f_{\text{esc}} \sim 0.35$ . Within the currently available data and photometry, both CIGALE and Dense Basis have significant errors of  $\sim 0.3$ – $0.4$  on their  $f_{\text{esc}}$ -value estimates for each *individual* object. To within the large individual model fitting errors in  $f_{\text{esc}}$ , the two different model estimates are thus broadly consistent, although not identical. For all galaxies, the range of median  $f_{\text{esc}}$ -values does suggest that the CIGALE and Dense Basis models imply escape fractions that may be high enough to reionize the Universe with these UV-bright galaxies (Finkelstein et al. 2012; Robertson et al. 2015; Naidu et al. 2020).

Fig. 5 shows comparisons between model parameters for the 13 galaxies and uses their  $f_{\text{esc}}$ -values as corrected using the linear fits in Fig. 3. Fig. 5a shows the  $z \simeq 0$  relation between  $E_{B-V}$  and  $\beta$  using the equations that Meurer et al. (1999) and Calzetti et al. (2000) found at

$z \simeq 0$ . The  $z \simeq 6$  galaxies of our sample have bluer  $\beta$ -values than local galaxies at a given extinction level by about  $-0.4$  in  $\beta$ -value. This is in line with expectations, and observations that these galaxies at  $z \simeq 6$  are bluer given their particularly younger stellar populations (e.g., Bouwens et al. 2014; Labbé et al. 2010). Fig. 5b shows the relationship between implied  $f_{\text{esc}}$  and  $\beta$ , and Fig. 5c shows the relationship between implied  $f_{\text{esc}}$  and  $E_{B-V}$ . Fig. 5d and e show the same as Fig. 5b and c, but using the Dense Basis  $f_{\text{esc}}$ -values instead. The Dense Base models did not consider  $\beta$ -values and assumed  $E_{B-V} \simeq 0.2$  mag, and so only the distribution over their  $f_{\text{esc}}$ -values is shown. No strong trends can be seen between  $f_{\text{esc}}$  and  $E_{B-V}$  nor  $f_{\text{esc}}$  and  $\beta$ .

#### 4. ANALYSIS OF THE SED MODELS FOR THE 13 SDF GALAXIES AT $Z \simeq 6$

The sample of 13 SDF galaxies at  $z \simeq 6$  help to constrain which galaxy population(s) could have completed and maintained reionization of the Universe at  $z \simeq 6$ . Fig. 4 shows cumulative distributions and Gaussians of two subsamples of the 13 galaxies with the most reliable  $f_{\text{esc}}$  estimates: bluer galaxies ( $\beta < -2.35$ ) and redder galaxies ( $\beta$ -values  $\geq -2.35$ ). Fig. 4a and b show that the bluer subsample has its distribution peaking around  $\beta \simeq -2.6$ , while the redder subsample has its distribution peaking around  $\beta \simeq -2.2$ . Fig. 4c and d show that the bluer subsample has lower implied  $E_{B-V}$ -values with a median  $E_{B-V} \simeq 0$  mag, while the redder subsample has a higher median near  $E_{B-V} \simeq 0.05$  mag. Finally, Fig. 4e and f show that the bluer subsample has smaller implied  $f_{\text{esc}}$ -values, with a mode and median of around  $f_{\text{esc}} \simeq 0$ , while the redder subsample has larger implied  $f_{\text{esc}}$ -values of  $f_{\text{esc}} \simeq 0.5$ .

Fig. 5b and c shows that our sample galaxies have large uncertainties and range in the implied  $f_{\text{esc}}$ -values ( $\sim 0.1$ – $0.35$ ). Thus, there may be some overlap between the low and high implied  $f_{\text{esc}}$  galaxies presented in Fig. 5. While large photometric and modeling uncertainties result in large uncertainties in the implied model escape fraction values, our analysis does suggest that  $f_{\text{esc}}$  for  $z \sim 6$  galaxies is likely less than 0.8 in general. In fact, our analysis of 13 independent objects with two independent SED-fitting codes suggests that  $f_{\text{esc}}$ -values around 0.5 are most typical of bright  $z \sim 6$  galaxies. This is consistent with the  $f_{\text{esc}}$ -values necessary for bright objects to reionize the Universe by  $z \sim 6$  (Finkelstein et al. 2012; Robertson et al. 2015; Naidu et al. 2020).

Fig 5a indicates that bluer implied  $\beta$  corresponds with lower implied  $E_{B-V}$  values. At given CIGALE-fit  $E_{B-V}$  values, the implied  $\beta$ -values at  $z \simeq 6$  seem to be steeper than those at  $z \simeq 0$  found from the Calzetti/Meurer relation (Calzetti et al. 2000; Meurer et al. 1999) by about  $-0.4$  in  $\beta$ . This is expected, and agrees with observations (e.g., Bouwens et al. 2014; Labbé et al. 2010), since higher redshift galaxies tend to have younger stellar populations and lower metallicity and extinction, and therefore bluer UV-continuum than low redshift galaxies.

Fig. 5b and 5c do not show strong trends between the parameters. At best, very weak relationships can be seen between redder  $\beta$  or  $E_{B-V}$  with lower  $f_{\text{esc}}$ . Fig. 5d and e using the Dense Basis  $f_{\text{esc}}$ -values do not show any significant trends. This suggests that some other factors besides nebular emission or dust extinction may contribute to LyC escaping the galaxies.

One concern was that CIGALE produced larger  $f_{\text{esc}}$  with redder  $\beta$  because it could not distinguish between young galaxies with strong line emission and mature ones with a larger Balmer break. Misidentifying more mature galaxies as younger ones could overestimate the line fluxes from the contribution of the Balmer break, inflating  $f_{\text{esc}}$ . To test if this problem truly existed, a single galaxy was modeled multiple times, but each with flux values slightly shifted with random values within uncertainty. If CIGALE did not distinguish the two sets of galaxies, lower  $f_{\text{esc}}$  should always have yielded steeper  $\beta$ -values. However, this was not always the case, as some models with lower  $f_{\text{esc}}$  had higher  $\beta$  than models with higher  $f_{\text{esc}}$ . In conclusion, there thus seem to be mild correlations at  $z \simeq 6$  between the CIGALE model  $f_{\text{esc}}$ ,  $\beta$ , and  $E_{B-V}$  -values, in the sense that the implied  $f_{\text{esc}}$  may trend to higher values for both redder model  $\beta$  and for higher model  $E_{B-V}$  values.

A range of  $f_{\text{esc}}$ -values is possible for any  $\beta$  or  $E_{B-V}$  value for both CIGALE and Dense Basis values. Together with the general lack of clear trends between  $f_{\text{esc}}$  and  $\beta$ - or  $E_{B-V}$  -values discussed above, the escape fraction of these galaxies then may depend on some other factors, such as the geometry or viewing angle, and the porosity of its ISM (see e.g., Smith et al. 2018), that may allow certain lines-of-sight *into the galaxy* to provide higher LyC escape fractions than others (Ma et al. 2020), and not so much the physical properties of the galaxies. When deeper data over a wider wavelength range becomes available with JWST, the average opening angle of the outflow geometry may then be estimated from the median  $f_{\text{esc}} \sim 0.3\text{--}0.55$  implied by the CIGALE models in the current work, which is the  $f_{\text{esc}}$ -value needed to complete and maintain the reionization of the Universe

at  $z \simeq 6$ . Cosmological simulations have found that spikes in  $f_{\text{esc}}$  come after star-formation episodes, which may indicate channels through the ISM must first be cleared for LyC to escape (e.g., Smith et al. 2019). Because these phenomena that create the ISM openings may differ for individual galaxies, a large range of  $f_{\text{esc}}$  could then be produced, as our figures suggest.

## 5. SUMMARY

We extended the SED modeling and choose a more robust sample of  $z \simeq 6$  Ly $\alpha$  emitting galaxies within the Subaru Deep Field with detailed SED analyses from 7 Jiang et al. (2020) to 13. Each of these galaxies had extant ground- and space-based optical-IR observations of sufficient quality and depth to constrain their SEDs. All SED fitting was performed here using the CIGALE package (Boquien et al. 2019). Using the best-fitting CIGALE SED models, we investigated trends between physical parameters, such as the fitted UV-slope,  $\beta$ , the fitted extinction,  $E_{B-V}$ , and the implied escape fractions ( $f_{\text{esc}}$ ) to infer what factors may have affected reionization at  $z \simeq 6$ .

For our sample of 13 galaxies, the implied ages of the galaxies with uncertainty ranged from 30 to 800 Myr, and the implied metallicity from 0.0001 to 0.03, indicating that a wide range of parameter values is possible for galaxies with blue  $\beta$  at  $z \simeq 6$ . We found that galaxies at  $z \simeq 6$  may have a median escape fraction as implied by CIGALE and Dense Basis of  $f_{\text{esc}} \sim 0.35\text{--}0.55$ . The SED fits and  $f_{\text{esc}}$ -values may be improved with deeper observations over a wider wavelength range, such as with the JWST, to improve the SED models. Furthermore, the implied  $\beta$ -values were steeper at given model  $E_{B-V}$  values for  $z \simeq 6$  galaxies, when compared to galaxies at  $z \simeq 0$ , as found by Calzetti et al. (e.g., 2000) and Meurer et al. (1999).

No significant trends were found between  $f_{\text{esc}}$  and rest of the parameters, given the significant uncertainties in the data and the modeling. To better constrain the CIGALE and Dense Basis models, more accurate data and spectroscopic observations further into the infrared range will be needed. Currently, only shallow *Spitzer* and *Herschel* data are available. Furthermore, the spectra of the galaxies, from which their redshift were derived, does not cover a wide-enough wavelength range to provide additional constraints to the available broadband data for better SED fitting. Future deeper spectral observations, such as with *JWST* NIRSpec at 1–5  $\mu\text{m}$ , would provide much better constraints to their SED parameters. At  $z \simeq 6$ , the *JWST*/NIRSpec will be able to observe H $\beta$  and [OIII] emission lines at 3.0–3.5

$\mu\text{m}$ , which will provide much better constraints on the CIGALE models than using broadband fluxes alone.

**We note that besides the high uncertainty in our results, we also assumed that we’ve correctly modeled the  $\text{Ly}\alpha$  lines for these galaxies. While we have attempted to correct for this assumption by increasing the uncertainties of filters with  $\text{Ly}\alpha$  contribution in the modeling, future observations are needed to produce more reliable results.**

Another way to approach this problem will be to use the available spectra to estimate the physical parameters of these galaxies at  $z \simeq 6$ . The quality of the spectra will have to be high to make such estimates possible, and to make a better comparison between the CIGALE models and the available data. With higher accuracy data and spectroscopy further into the infrared, the characteristics of galaxies with steep  $\beta$  and the escape fractions of high redshift galaxies can be better characterized to more fully constrain the sources of the reionization of the Universe at  $z \simeq 6$ .

#### ACKNOWLEDGMENTS

We thank the two anonymous referees; their reports helped us clarify and significantly improve our manuscript, and pointed us to the Anderson-Darling test. We also thank Ian Smail, Pratika Dayal, Eric Gawiser and Claudia Scarlata for helpful suggestions and several relevant references. Based on observations made with the NASA/ESA Hubble Space Telescope, obtained at the Space Telescope Science Institute. Support for HST program GO15137 was provided by NASA through a grant from the Space Telescope Science Institute, which is operated by the Association of Universities for Research in Astronomy, Inc., under NASA contract NAS 5-26555. RAW acknowledges support from NASA *JWST* Interdisciplinary Scientist grants NAG5-12460, NNX14AN10G and 80NSSC18K0200 from GSFC.

*Facilities:* *HST*(ACS, WFC3/UVIS, WFC3/IR), Subaru(HSC), *Spitzer*/IRAC, UKIRT/WFCAM

*Software:* *astropy* (Astropy Collaboration et al. 2018), CIGALE (Boquien et al. 2019)

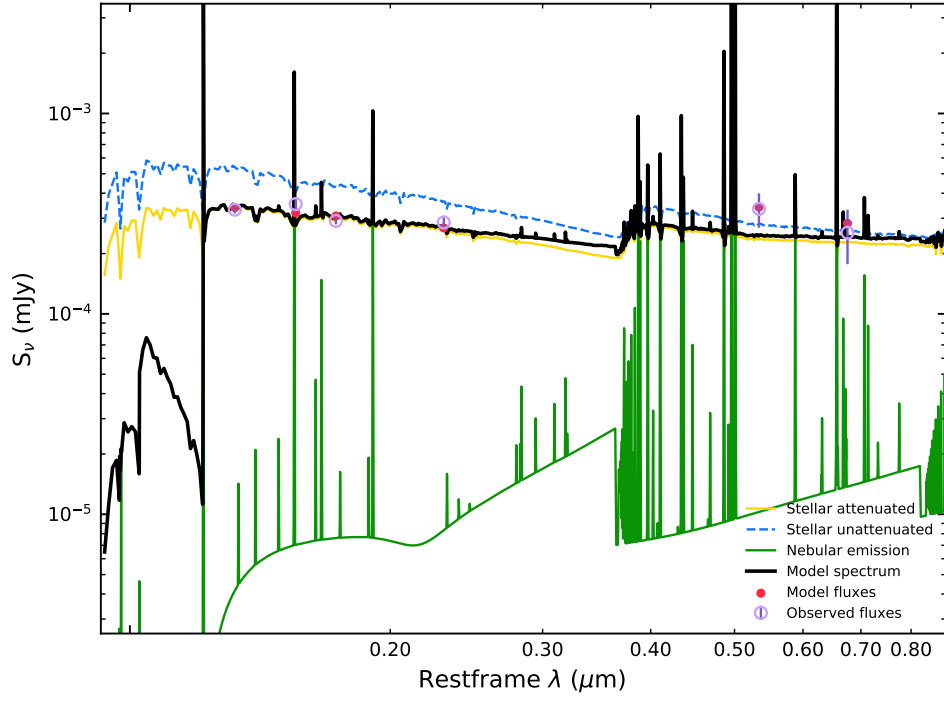
## REFERENCES

- Astropy Collaboration, Price-Whelan, A. M., SipHocz, B. M., et al. 2018, *aj*, 156, 123, doi: [10.3847/1538-3881/aabc4f](https://doi.org/10.3847/1538-3881/aabc4f)
- Barrow, K. S. S., Robertson, B. E., Ellis, R. S., et al. 2020, *ApJL*, 902, L39, doi: [10.3847/2041-8213/abbd8e](https://doi.org/10.3847/2041-8213/abbd8e)
- Bertin, E., & Arnouts, S. 1996, *A&AS*, 117, 393, doi: [10.1051/aas:1996164](https://doi.org/10.1051/aas:1996164)
- Bian, F., & Fan, X. 2020, *MNRAS*, 493, L65, doi: [10.1093/mnras/slaa007](https://doi.org/10.1093/mnras/slaa007)
- Boquien, M., Burgarella, D., Roehlly, Y., et al. 2019, *A&A*, 622, A103, doi: [10.1051/0004-6361/201834156](https://doi.org/10.1051/0004-6361/201834156)
- Bouwens, R. J., Illingworth, G. D., Oesch, P. A., et al. 2014, *ApJ*, 793, 115, doi: [10.1088/0004-637X/793/2/115](https://doi.org/10.1088/0004-637X/793/2/115)
- . 2015, *ApJ*, 803, 34, doi: [10.1088/0004-637X/803/1/34](https://doi.org/10.1088/0004-637X/803/1/34)
- Calzetti, D., Armus, L., Bohlin, R. C., et al. 2000, *ApJ*, 533, 682, doi: [10.1086/308692](https://doi.org/10.1086/308692)
- Conroy, C. 2013, *ARA&A*, 51, 393, doi: [10.1146/annurev-astro-082812-141017](https://doi.org/10.1146/annurev-astro-082812-141017)
- Ellis, R. S., McLure, R. J., Dunlop, J. S., et al. 2013, *ApJL*, 763, L7, doi: [10.1088/2041-8205/763/1/L7](https://doi.org/10.1088/2041-8205/763/1/L7)
- Finkelstein, S. L., Papovich, C., Ryan, R. E., et al. 2012, *ApJ*, 758, 93, doi: [10.1088/0004-637X/758/2/93](https://doi.org/10.1088/0004-637X/758/2/93)
- Finkelstein, S. L., Papovich, C., Dickinson, M., et al. 2013, *Nature*, 502, 524, doi: [10.1038/nature12657](https://doi.org/10.1038/nature12657)
- Finkelstein, S. L., D’Aloisio, A., Paardekooper, J.-P., et al. 2019, *ApJ*, 879, 36, doi: [10.3847/1538-4357/ab1ea8](https://doi.org/10.3847/1538-4357/ab1ea8)
- Furusawa, H., Kosugi, G., Akiyama, M., et al. 2008, *ApJS*, 176, 1, doi: [10.1086/527321](https://doi.org/10.1086/527321)
- Gardner, J. P., Mather, J. C., Clampin, M., et al. 2006, *SSRv*, 123, 485, doi: [10.1007/s11214-006-8315-7](https://doi.org/10.1007/s11214-006-8315-7)
- Grogin, N. A., Kocevski, D. D., Faber, S. M., et al. 2011, *ApJS*, 197, 35, doi: [10.1088/0067-0049/197/2/35](https://doi.org/10.1088/0067-0049/197/2/35)
- Hayes, M., Schaerer, D., Östlin, G., et al. 2011, *ApJ*, 730, 8, doi: [10.1088/0004-637X/730/1/8](https://doi.org/10.1088/0004-637X/730/1/8)
- Hewett, P. C., Warren, S. J., Leggett, S. K., & Hodgkin, S. T. 2006, *MNRAS*, 367, 454, doi: [10.1111/j.1365-2966.2005.09969.x](https://doi.org/10.1111/j.1365-2966.2005.09969.x)
- Hodgkin, S. T., Irwin, M. J., Hewett, P. C., & Warren, S. J. 2009, *MNRAS*, 394, 675, doi: [10.1111/j.1365-2966.2008.14387.x](https://doi.org/10.1111/j.1365-2966.2008.14387.x)
- Hu, W., Wang, J., Zheng, Z.-Y., et al. 2019, *ApJ*, 886, 90, doi: [10.3847/1538-4357/ab4cf4](https://doi.org/10.3847/1538-4357/ab4cf4)
- Iyer, K., & Gawiser, E. 2017, *ApJ*, 838, 127, doi: [10.3847/1538-4357/aa63f0](https://doi.org/10.3847/1538-4357/aa63f0)
- Jiang, L., Cohen, S. H., Windhorst, R. A., et al. 2020, *ApJ*, 889, 90, doi: [10.3847/1538-4357/ab64ea](https://doi.org/10.3847/1538-4357/ab64ea)
- Jiang, L., Egami, E., Mechtley, M., et al. 2013, *ApJ*, 772, 99, doi: [10.1088/0004-637X/772/2/99](https://doi.org/10.1088/0004-637X/772/2/99)
- Jiang, L., Finlator, K., Cohen, S. H., et al. 2016, *ApJ*, 816, 16, doi: [10.3847/0004-637X/816/1/16](https://doi.org/10.3847/0004-637X/816/1/16)
- Joye, W. A., & Mandel, E. 2003, in *Astronomical Society of the Pacific Conference Series*, Vol. 295, *Astronomical Data Analysis Software and Systems XII*, ed. H. E. Payne, R. I. Jedrzejewski, & R. N. Hook, 489
- Kashikawa, N., Shimasaku, K., Matsuda, Y., et al. 2011, *ApJ*, 734, 119, doi: [10.1088/0004-637X/734/2/119](https://doi.org/10.1088/0004-637X/734/2/119)
- Keating, L. C., Kulkarni, G., Haehnelt, M. G., Chardin, J., & Aubert, D. 2020, *MNRAS*, 497, 906, doi: [10.1093/mnras/staa1909](https://doi.org/10.1093/mnras/staa1909)
- Kim, D., Jansen, R. A., & Windhorst, R. A. 2017, *ApJ*, 840, 28, doi: [10.3847/1538-4357/aa6ba1](https://doi.org/10.3847/1538-4357/aa6ba1)
- Koekemoer, A. M., Faber, S. M., Ferguson, H. C., et al. 2011, *ApJS*, 197, 36, doi: [10.1088/0067-0049/197/2/36](https://doi.org/10.1088/0067-0049/197/2/36)
- Konno, A., Ouchi, M., Ono, Y., et al. 2014, *ApJ*, 797, 16, doi: [10.1088/0004-637X/797/1/16](https://doi.org/10.1088/0004-637X/797/1/16)
- Kotulla, R., Fritze, U., Weilbacher, P., & Anders, P. 2009, *MNRAS*, 396, 462, doi: [10.1111/j.1365-2966.2009.14717.x](https://doi.org/10.1111/j.1365-2966.2009.14717.x)
- Labbé, I., González, V., Bouwens, R. J., et al. 2010, *ApJL*, 716, L103, doi: [10.1088/2041-8205/716/2/L103](https://doi.org/10.1088/2041-8205/716/2/L103)
- Laporte, N., Ellis, R. S., Boone, F., et al. 2017, *ApJL*, 837, L21, doi: [10.3847/2041-8213/aa62aa](https://doi.org/10.3847/2041-8213/aa62aa)
- Lawrence, A., Warren, S. J., Almaini, O., et al. 2007, *MNRAS*, 379, 1599, doi: [10.1111/j.1365-2966.2007.12040.x](https://doi.org/10.1111/j.1365-2966.2007.12040.x)
- Loeb, A., & Barkana, R. 2001, *ARA&A*, 39, 19, doi: [10.1146/annurev.astro.39.1.19](https://doi.org/10.1146/annurev.astro.39.1.19)
- Lorenzoni, S., Bunker, A. J., Wilkins, S. M., et al. 2011, *MNRAS*, 414, 1455, doi: [10.1111/j.1365-2966.2011.18479.x](https://doi.org/10.1111/j.1365-2966.2011.18479.x)
- Ma, X., Quataert, E., Wetzell, A., et al. 2020, *MNRAS*, 498, 2001, doi: [10.1093/mnras/staa2404](https://doi.org/10.1093/mnras/staa2404)
- Maseda, M. V., Franx, M., Chevallard, J., & Curtis-Lake, E. 2019, *MNRAS*, 486, 3290, doi: [10.1093/mnras/stz818](https://doi.org/10.1093/mnras/stz818)
- McLure, R. J., Dunlop, J. S., de Ravel, L., et al. 2011, *MNRAS*, 418, 2074, doi: [10.1111/j.1365-2966.2011.19626.x](https://doi.org/10.1111/j.1365-2966.2011.19626.x)
- Meurer, G. R., Heckman, T. M., & Calzetti, D. 1999, *ApJ*, 521, 64, doi: [10.1086/307523](https://doi.org/10.1086/307523)
- Miralda-Escudé, J., Haehnelt, M., & Rees, M. J. 2000, *ApJ*, 530, 1, doi: [10.1086/308330](https://doi.org/10.1086/308330)
- Naidu, R. P., Tacchella, S., Mason, C. A., et al. 2020, *ApJ*, 892, 109, doi: [10.3847/1538-4357/ab7cc9](https://doi.org/10.3847/1538-4357/ab7cc9)
- Noll, S., Burgarella, D., Giovannoli, E., et al. 2009, *A&A*, 507, 1793, doi: [10.1051/0004-6361/200912497](https://doi.org/10.1051/0004-6361/200912497)
- Oesch, P. A., Labbé, I., Bouwens, R. J., et al. 2013, *ApJ*, 772, 136, doi: [10.1088/0004-637X/772/2/136](https://doi.org/10.1088/0004-637X/772/2/136)

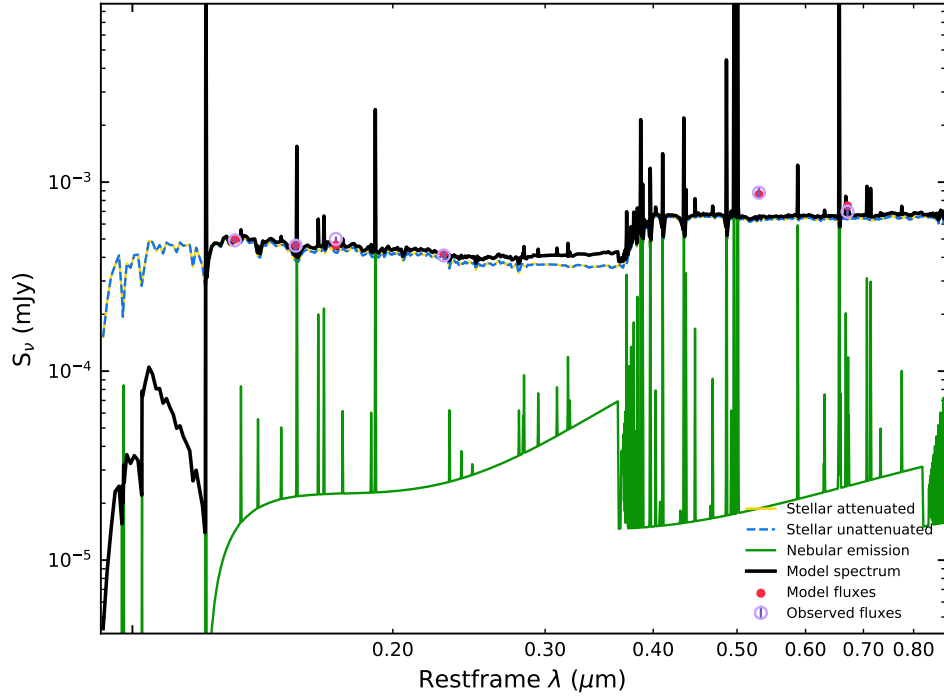
- Oke, J. B., & Gunn, J. E. 1983, *ApJ*, 266, 713, doi: [10.1086/160817](https://doi.org/10.1086/160817)
- Ono, Y., Ouchi, M., Shimasaku, K., et al. 2010, *ApJ*, 724, 1524, doi: [10.1088/0004-637X/724/2/1524](https://doi.org/10.1088/0004-637X/724/2/1524)
- Ota, K., Iye, M., Kashikawa, N., et al. 2017, *ApJ*, 844, 85, doi: [10.3847/1538-4357/aa7a0a](https://doi.org/10.3847/1538-4357/aa7a0a)
- Ouchi, M., Harikane, Y., Shibuya, T., et al. 2018, *PASJ*, 70, S13, doi: [10.1093/pasj/psx074](https://doi.org/10.1093/pasj/psx074)
- Papovich, C., Dickinson, M., & Ferguson, H. C. 2001, *ApJ*, 559, 620, doi: [10.1086/322412](https://doi.org/10.1086/322412)
- Robertson, B. E., Ellis, R. S., Furlanetto, S. R., & Dunlop, J. S. 2015, *ApJL*, 802, L19, doi: [10.1088/2041-8205/802/2/L19](https://doi.org/10.1088/2041-8205/802/2/L19)
- Ryan, R. E. 2011, iGalFit: An Interactive Tool for GalFit. <https://arxiv.org/abs/1110.1090>
- Schaerer, D., & de Barros, S. 2009, *A&A*, 502, 423, doi: [10.1051/0004-6361/200911781](https://doi.org/10.1051/0004-6361/200911781)
- Shapley, A. E., Steidel, C. C., Adelberger, K. L., et al. 2001, *ApJ*, 562, 95, doi: [10.1086/323432](https://doi.org/10.1086/323432)
- Shapley, A. E., Steidel, C. C., Erb, D. K., et al. 2005, *ApJ*, 626, 698, doi: [10.1086/429990](https://doi.org/10.1086/429990)
- Smith, A., Ma, X., Bromm, V., et al. 2019, *MNRAS*, 484, 39, doi: [10.1093/mnras/sty3483](https://doi.org/10.1093/mnras/sty3483)
- Smith, B. M., Windhorst, R. A., Jansen, R. A., et al. 2018, *ApJ*, 853, 191, doi: [10.3847/1538-4357/aaa3dc](https://doi.org/10.3847/1538-4357/aaa3dc)
- Smith, B. M., Windhorst, R. A., Cohen, S. H., et al. 2020, *ApJ*, 897, 41, doi: [10.3847/1538-4357/ab8811](https://doi.org/10.3847/1538-4357/ab8811)
- Stark, D. P., Ellis, R. S., Charlot, S., et al. 2017, *MNRAS*, 464, 469, doi: [10.1093/mnras/stw2233](https://doi.org/10.1093/mnras/stw2233)
- Steidel, C. C., Bogosavljević, M., Shapley, A. E., et al. 2018, *ApJ*, 869, 123, doi: [10.3847/1538-4357/aaed28](https://doi.org/10.3847/1538-4357/aaed28)
- Trenti, M., Bradley, L. D., Stiavelli, M., et al. 2011, *ApJL*, 727, L39, doi: [10.1088/2041-8205/727/2/L39](https://doi.org/10.1088/2041-8205/727/2/L39)
- Windhorst, R. A., Timmes, F. X., Wyithe, J. S. B., et al. 2018, *ApJS*, 234, 41, doi: [10.3847/1538-4365/aaa760](https://doi.org/10.3847/1538-4365/aaa760)
- Yan, H.-J., Windhorst, R. A., Hathi, N. P., et al. 2010, *Research in Astronomy and Astrophysics*, 10, 867, doi: [10.1088/1674-4527/10/9/003](https://doi.org/10.1088/1674-4527/10/9/003)



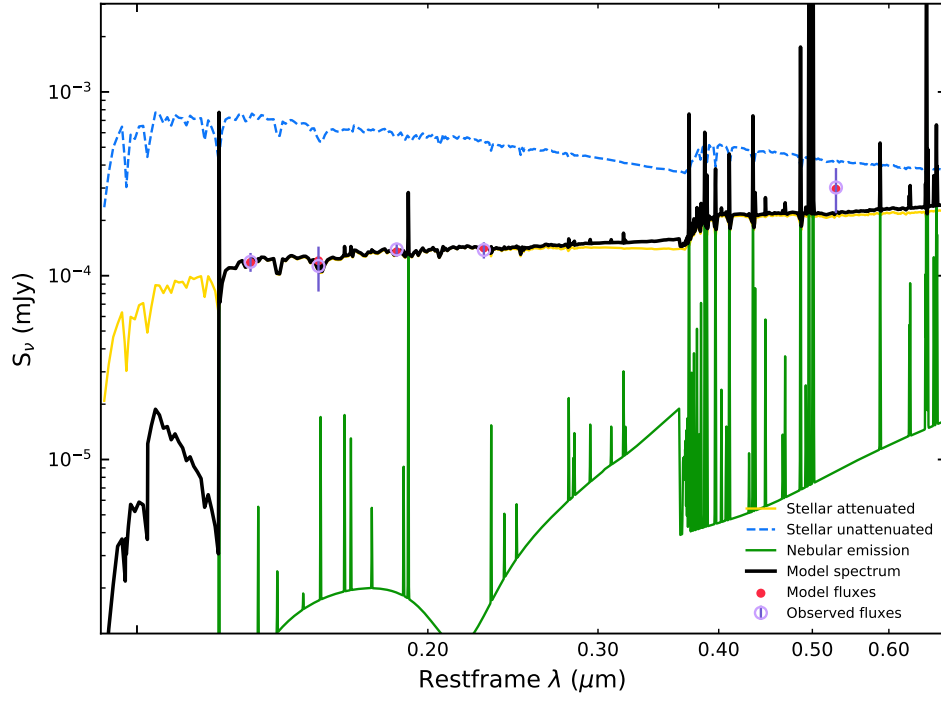




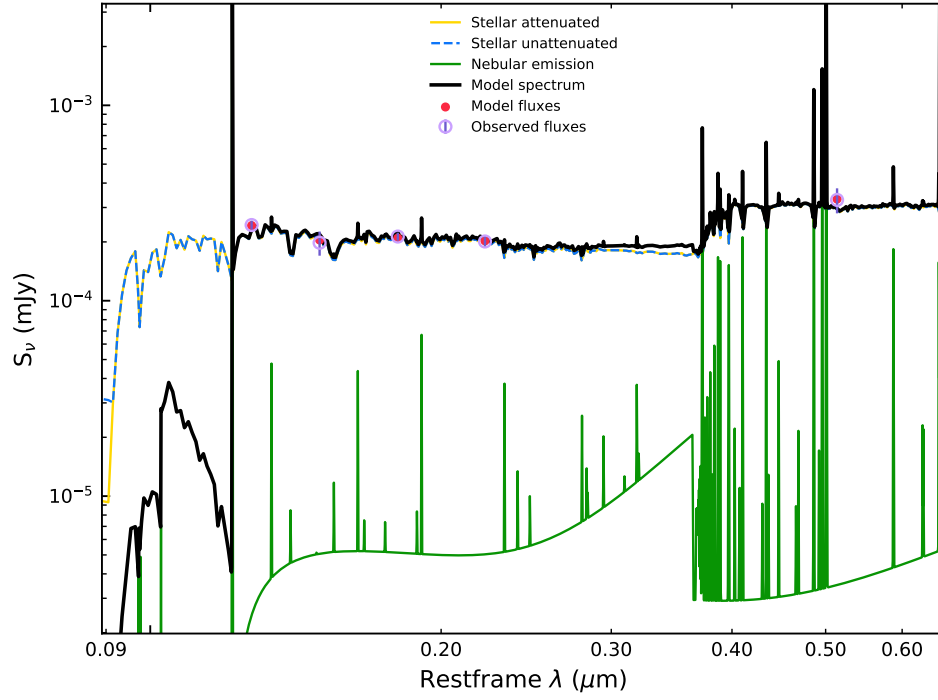
(ID03)



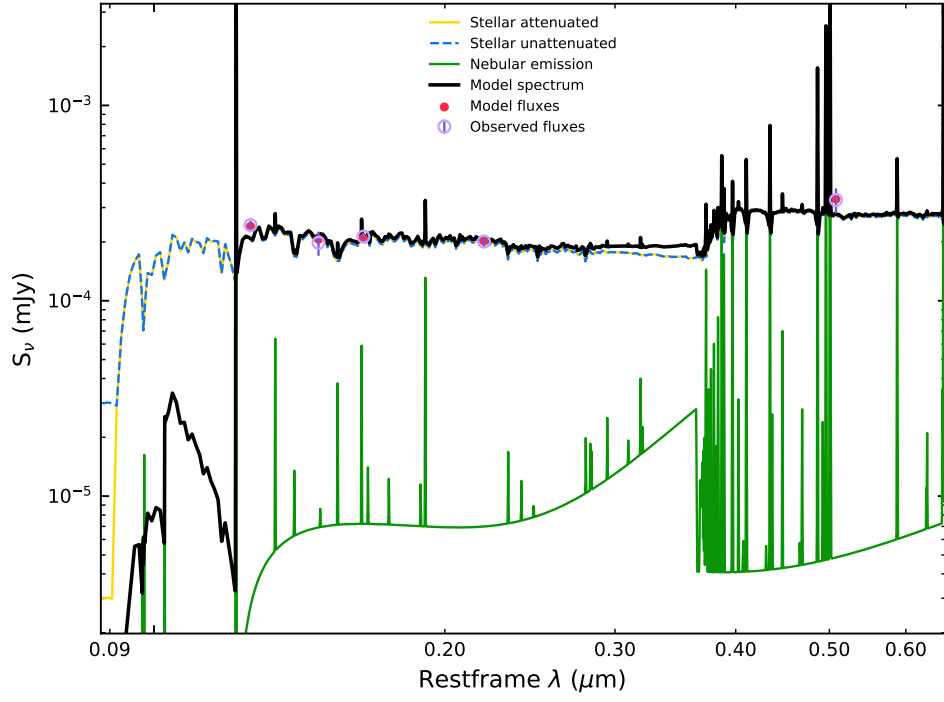
(ID15)



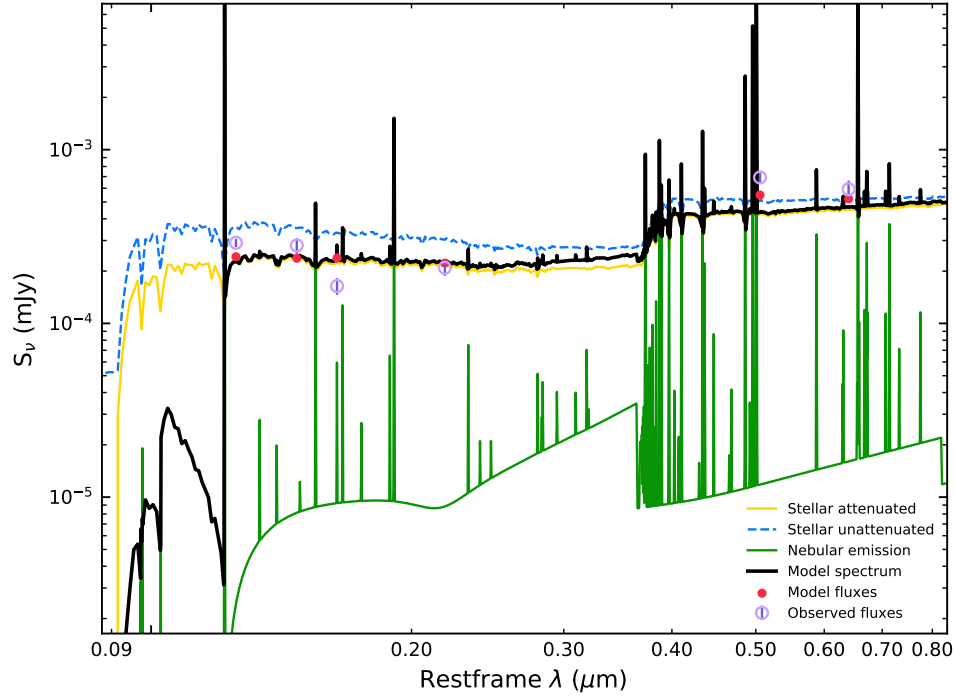
(ID20)



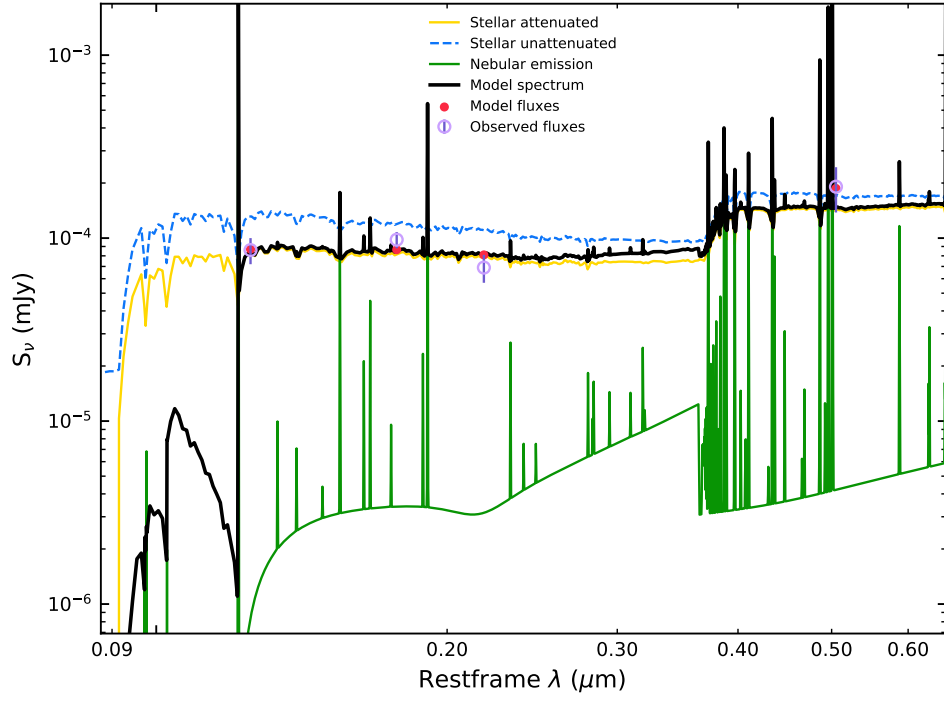
(ID23)



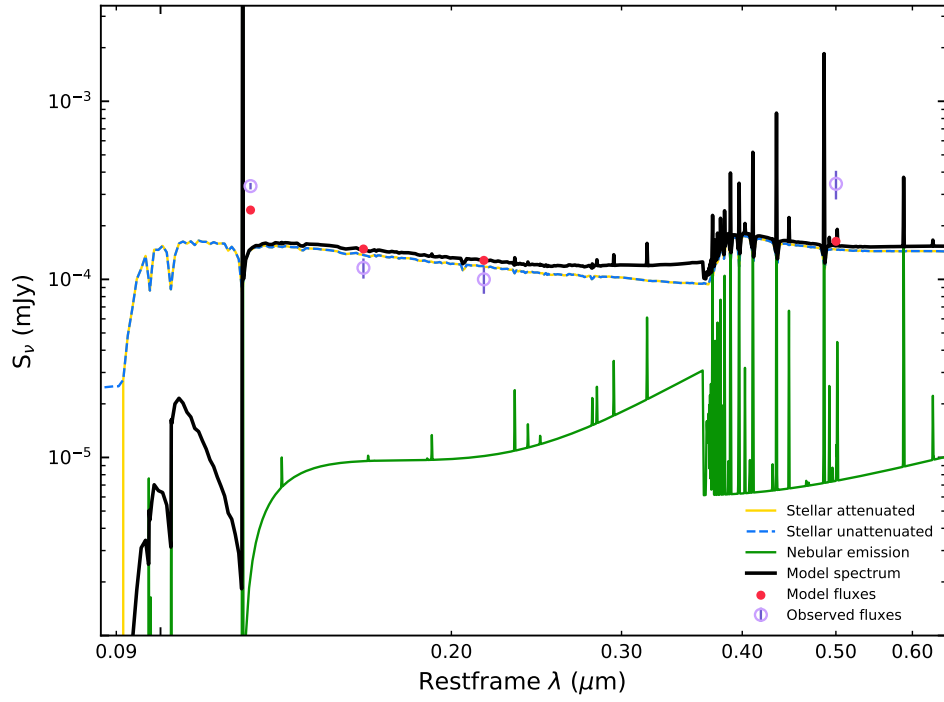
(ID24)



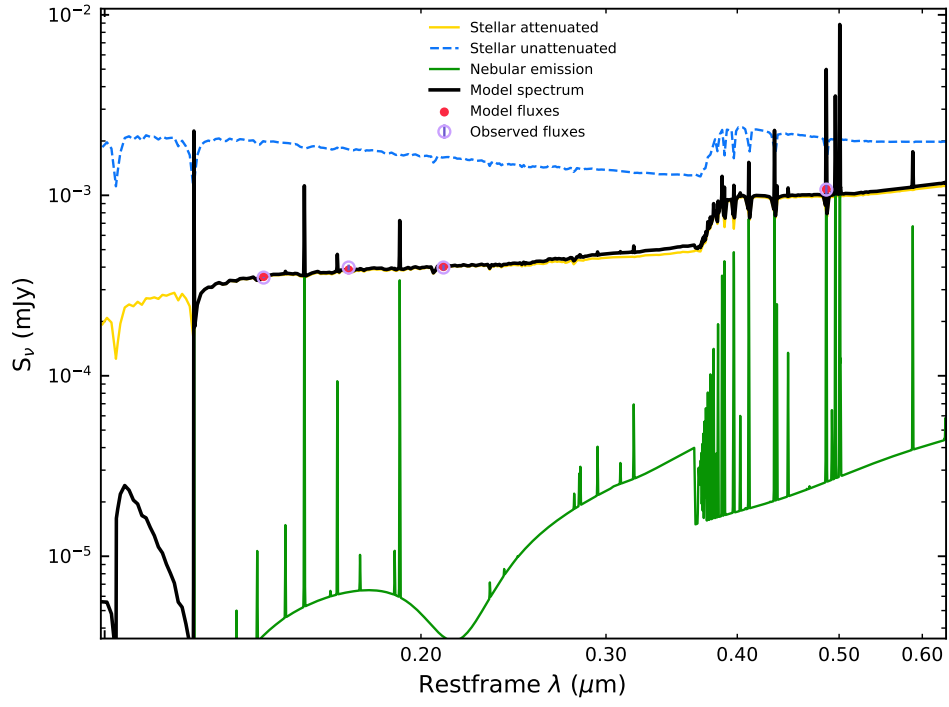
(ID25)



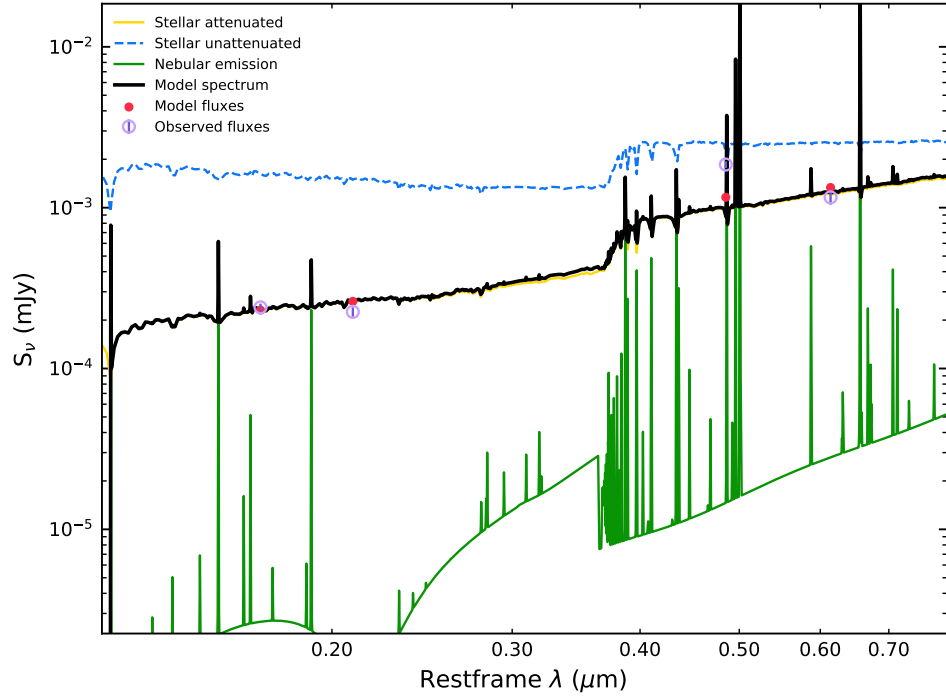
(ID27)



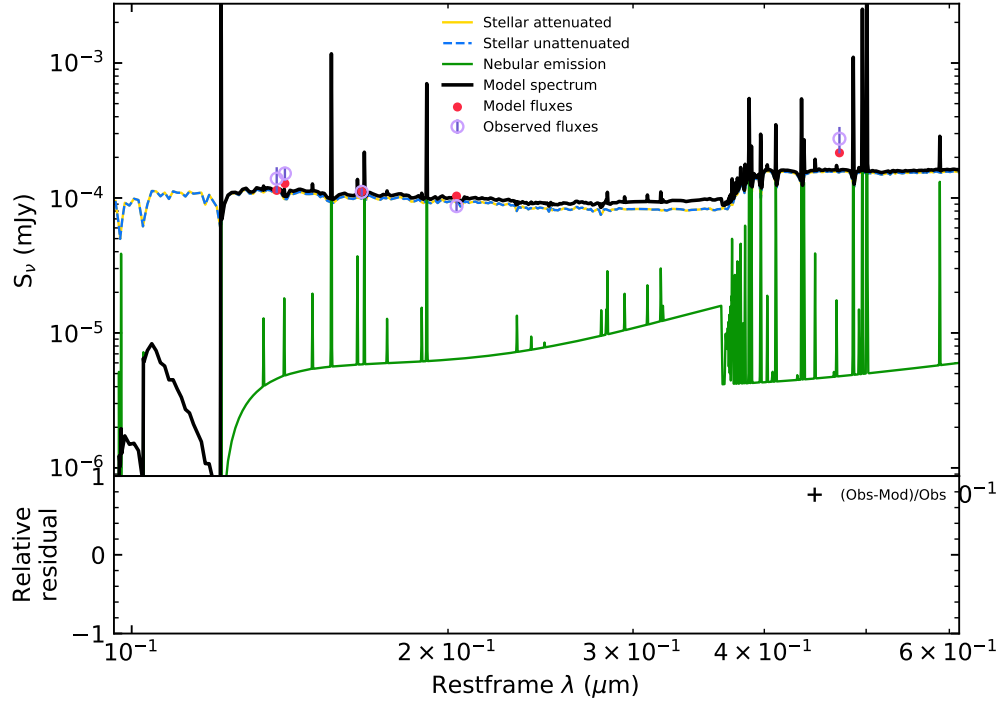
(ID31)



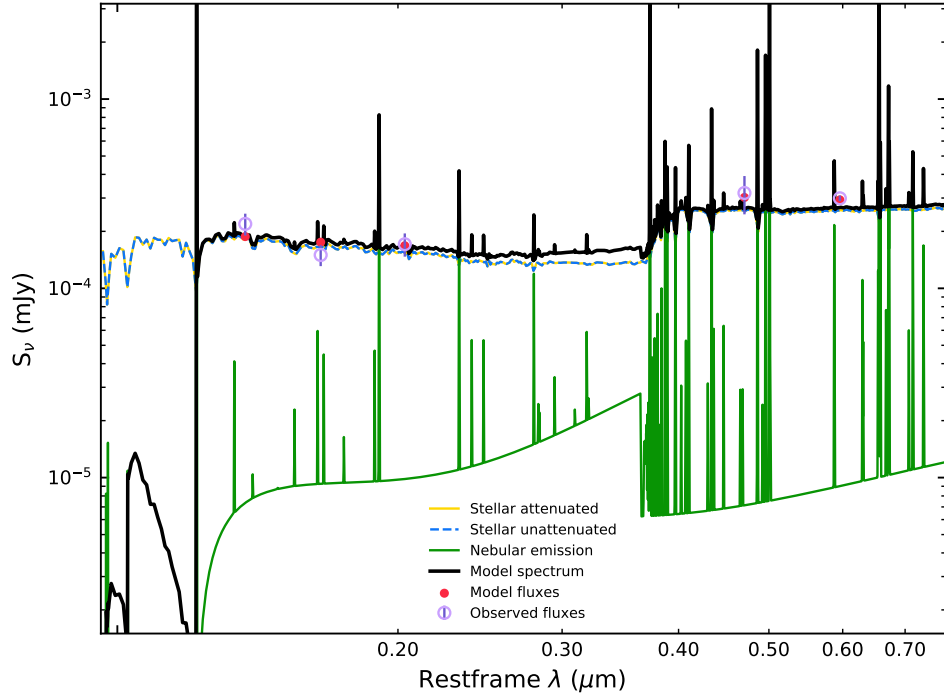
(ID34)



(ID35)

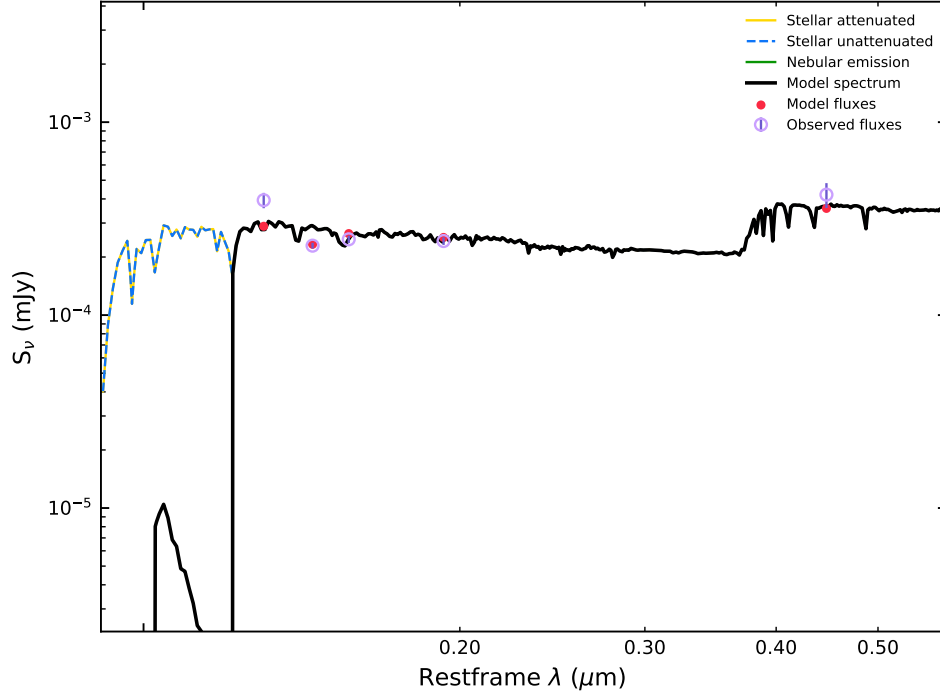


(ID43)



(ID54)





(ID62)

**Fig. Set 1. SED Models of the 13 galaxies**

**Figure 1.** The best-fit SED models of the 13 galaxies created using CIGALE (Boquien et al. 2019). The blue boxes are the observed fluxes while the red circles are the model fluxes. The uncertainties plotted are the  $3\sigma$  uncertainties. In general, the models are able to fit the observations, providing meaningful constraints on the extinction, UV-slope  $\beta$ , and escape fraction. Furthermore, the models produce redder implied slopes than J20.

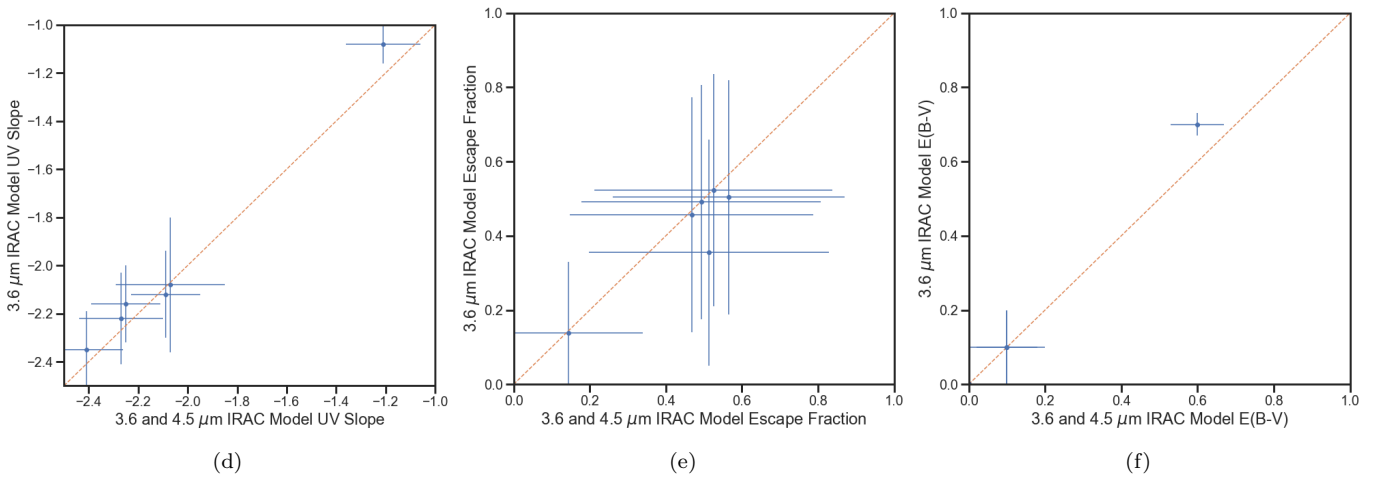


**Figure 2.** Comparison of  $\beta$ ,  $f_{\text{esc}}$ , and  $E_{B-V}$  of the models fit when both 3.6 and 4.5  $\mu\text{m}$  IRAC filters are included and when only 3.6  $\mu\text{m}$  is included, using the data of Tables 2 – 3. Only minor differences can be seen in the two sets of models, showing that the addition of the much noisier IRAC2 4.5  $\mu\text{m}$  data points does not affect the modeling significantly.

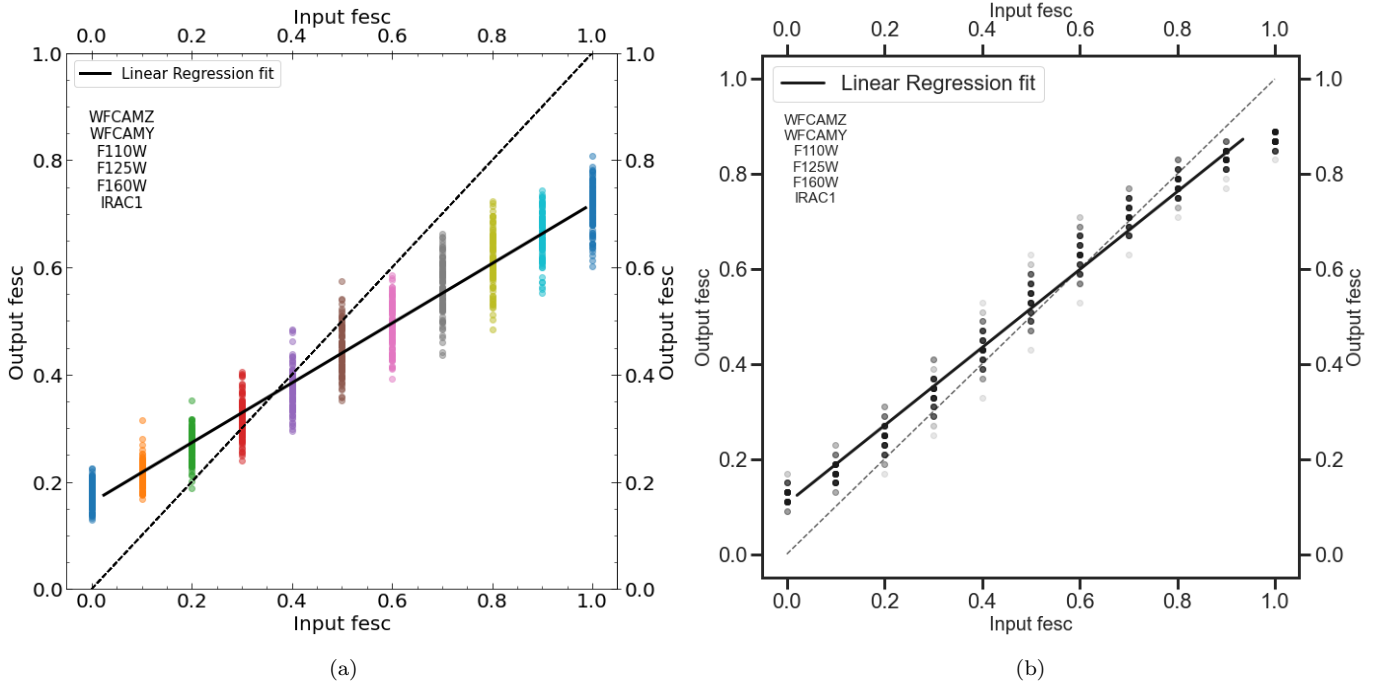


**Figure 3.** (a) [Left panel]: Output escape fraction using the CIGALE models against a range of input escape fractions. This was done by refitting 100 random variations of the original models with a fixed escape fraction created by CIGALE using the photometry in all filters plus its errors, but excluding the IRAC2 and K-band filters, which had the lowest S/N-ratio and did not constrain the SED fits well. The linear regression fit has an equation of  $f_{\text{esc},in} = 1.79f_{\text{esc},out} - 0.29$  (b) [Right panel]: Same as (a) for Dense Basis. Both panels show similar but not identical relationships between the input and output  $f_{\text{esc}}$ -values. We use the plotted linear regression fits to map the most likely output  $f_{\text{esc}}$ -values onto the input  $f_{\text{esc}}$ -values for both CIGALE and Dense Basis, thus correcting both modeling methods for this bias. The linear regression fit has an equation of  $f_{\text{esc},in} = 1.22f_{\text{esc},out} - 0.13$

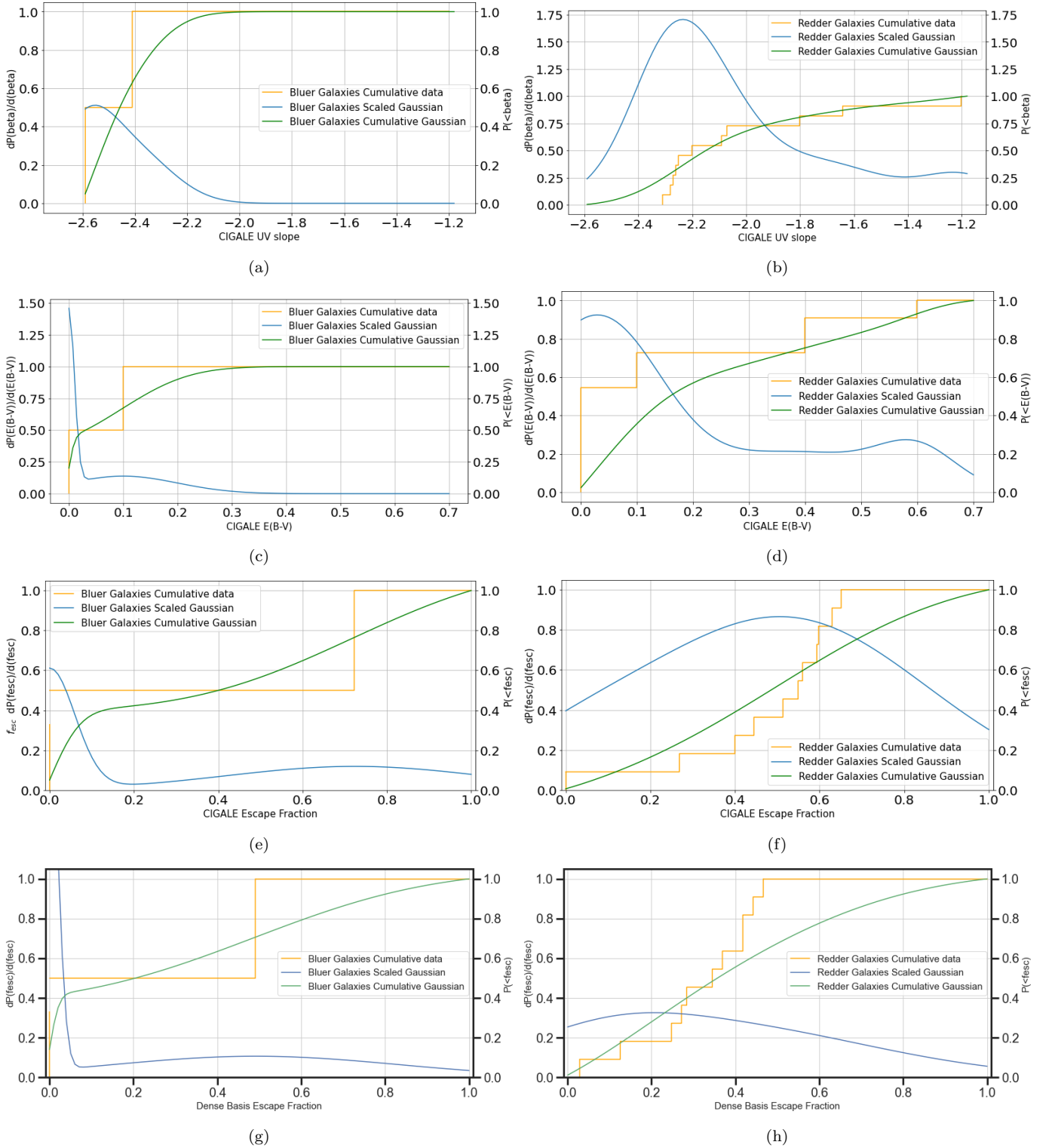


**Figure 4.** Distributions of the implied Bayesian UV-slope and escape fraction, and best-fit  $E_{B-V}$  lines of the 13 galaxies. The sample is divided into bluer galaxies with model  $\beta < -2.35$  and redder galaxies with model  $\beta \geq -2.35$ . Panels (g) and (h) show the distribution of the Dense Basis  $f_{\text{esc}}$ -values. The orange lines show the cumulative distributions of the individual adopted values with the probability shown on the right axis. The blue and green lines respectively show the scaled stacked model likelihoods and stacked cumulative distributions with probability for the latter on the left axis, assuming that the likelihood of the model parameter is normally distributed with the given mean and standard deviation. The CIGALE plots show that bluer galaxies — as selected — are more likely to have lower values of  $f_{\text{esc}}$  and lower  $E_{B-V}$ . (The Dense Base models did not consider  $\beta$ -values and assumed  $E_{B-V} \simeq 0.2$  mag, and so only the distribution over their  $f_{\text{esc}}$ -values is shown).

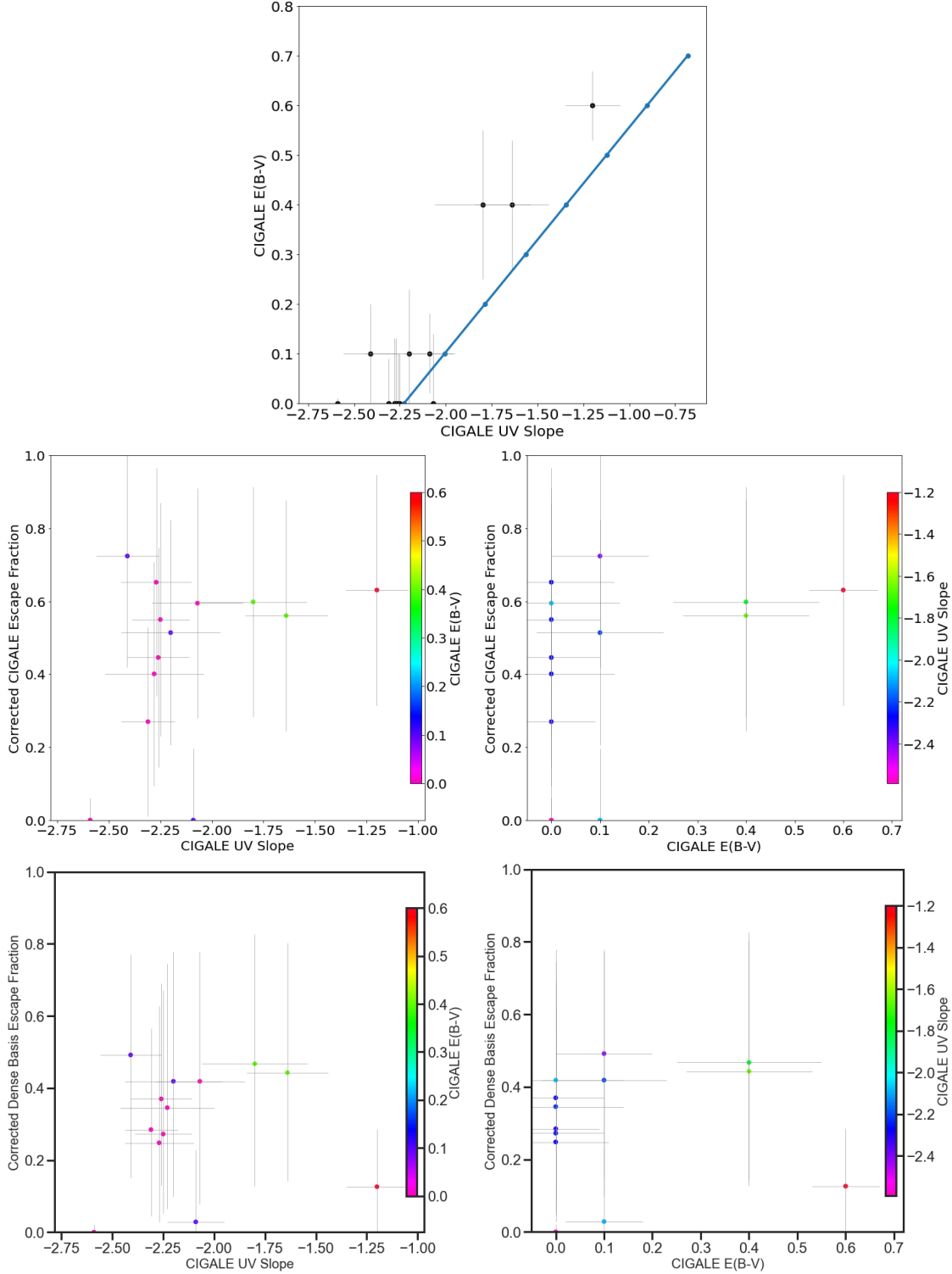


**Figure 5.** Distribution of the Bayesian  $\beta$  and  $f_{\text{esc}}$ , and best-fit  $E_{B-V}$  for the 13 galaxies. **(a) [Top panel]:** Best fit CIGALE  $E_{B-V}$  vs.  $\beta$ , which tends to be steeper (bluer) for lower implied  $E_{B-V}$  values. The local relation between  $E_{B-V}$  and  $\beta$  from Calzetti et al. (2000); Meurer et al. (1999) is plotted in blue, showing shallower  $\beta$ -values at  $z \simeq 0$  compared to our SDF sample at  $z \simeq 6$ . **(b),(c) [Middle panels]:** CIGALE  $f_{\text{esc}}$ -values as derived from the linear fit of Fig. 3. **(d),(e) [Bottom panels]:** Dense Basis  $f_{\text{esc}}$ -values as derived from the linear fit of Fig. 3. These figures suggest that the possible range of  $f_{\text{esc}}$  is between 0 to 0.8 with a median of **0.35–0.55**. No significant trends between  $f_{\text{esc}}$  and UV-slope or  $E_{B-V}$  are present. If the nebular emission or the dust extinction has no discernible effect on  $f_{\text{esc}}$ , other factors such as the distribution of holes vacated in the ISM by supernovae and/or weak AGN somewhat later in a galaxy’s evolutionary stage may be needed to let LyC radiation escape.